

Article

Process Improvements for Direct Reduced Iron Melting in the Electric Arc Furnace with Emphasis on Slag Operation

Marcus Kirschen ^{1,*}, Thomas Hay ² and Thomas Echterhof ²¹ Thermal Process Engineering, University of Bayreuth, Universitätsstrasse 30, D-94557 Bayreuth, Germany² Department for Industrial Furnaces and Heat Engineering, RWTH Aachen University, D-52074 Aachen, Germany; hay@iob.rwth-aachen.de (T.H.); echterhof@iob.rwth-aachen.de (T.E.)

* Correspondence: marcus.kirschen@uni-bayreuth.de

Abstract: Steelmaking based on direct reduced iron (DRI, and its compacted derivative hot briquetted iron, HBI) is an anticipated important global alternative to current steel production based on FeO_x reduction in blast furnaces due to its lower specific CO₂ emission. The majority of DRI is melted and refined in the electric arc furnace with different process conditions compared to the melting of steel scrap due to its raw material composition being rather different. We provide data and analysis of slag composition of DRI charges vs. steel scrap charges for 16 industrial electric arc furnaces (EAFs). Suggestions for optimized slag operation and resulting process improvements of DRI melting in the EAF are given. A dynamic mass and energy model of the DRI melting in the EAF is introduced to illustrate the implications of the adapted slag operation on the EAF process with DRI charges.

Keywords: electric arc furnace; direct reduced iron; process model; process improvement

Citation: Kirschen, M.; Hay, T.; Echterhof, T. Process Improvements for Direct Reduced Iron Melting in the Electric Arc Furnace with Emphasis on Slag Operation. *Processes* **2021**, *9*, 402. <https://doi.org/10.3390/pr9020402>

Received: 26 January 2021

Accepted: 18 February 2021

Published: 23 February 2021

Publisher's Note: MDPI stays neutral with regard to jurisdictional claims in published maps and institutional affiliations.



Copyright: © 2021 by the authors. Licensee MDPI, Basel, Switzerland. This article is an open access article distributed under the terms and conditions of the Creative Commons Attribution (CC BY) license (<http://creativecommons.org/licenses/by/4.0/>).

1. Introduction

The global steel industry is subject to significant changes in order to decrease its CO₂ emission representing the most important contribution within the production industry sector to global CO₂ emission, approximately 7%. Current steel production routes are mainly (1) ore reduction in the blast furnace and steel refining in the basic oxygen converter (BF-BOF) and (2) melting of steel scrap in the electric arc furnace (EAF) with CO₂ emissions in the range 1.6–2.2 tCO₂/tLS (BF-BOF) and 0.25–1.1 tCO₂/tLS (EAF), respectively [1–3]. An established alternative to coal and coke-based reduction of iron ores in blast furnaces is the ore reduction by coal or reformed natural gas (CO, H₂) to direct reduced iron (DRI) or hot briquetted iron (HBI) in shaft furnaces [4–6], rotary kilns [7–10] or rotary hearth furnaces [11]. The reduction of solid pellets is mainly realized at temperatures below melting, 900–1100 °C. With increased energy input and adapted reactor design, however, tapping of liquid iron is also possible [12,13]. Specific CO₂ emission figures are in the range 0.5–0.7 tCO₂/tDRI [14,15] due to the lower reactor temperature and natural gas-derived process gas as an energy source and ore reducing agent.

Global DRI/HBI production surpassed 108 million tons in 2019 [16], with a significant potential to replace coal-based iron making in blast furnaces globally. Iron ore reduction by hydrogen only has already been realized by applying reformed natural gas with shift reactor and CO₂ removal unit [5,17] but closed due to technical and commercial reasons. New concepts for carbon-free DRI production are available [18]. Generally, the total FeO content of ore grades for DRI production, FeO_{tot} > 65%, is higher than typical ore grades applied to the BF, FeO_{tot} < 65%. Today, the majority of DRI/HBI is melted with a varying share of steel scrap in EAFs with specific CO₂ emission figures in the range of 0.9 to 1.8 tCO₂/tLS (including local CO₂ intensity of electrical energy for EAF) [19,20].

2. Process Characteristics of DRI/HBI Melting and Refining in the EAF

The EAF production characteristics with high shares of DRI/HBI are, however, rather different from conventional melting of steel scrap due to the remaining 4–7 wt % gangue oxides and 1.5–4.3 wt % carbon (Table 1). If high amounts of DRI are charged continuously to the EAF, different power programs and adapted additions of lime, dolomitic lime or doloma are required.

Table 1. Typical direct reduced iron (DRI) compositions (in wt %).

Prod. Site	C	Fe _{met}	MgO	CaO	SiO ₂	Al ₂ O ₃	Metallization ¹
A	2.0	88.4	2.0	0.7	3.7	0.5	81.5
B	1.8	91.4	0.3	0.4	2.4	0.9	95.1
C	1.7	80.5	1.5	n.a.	3.1	0.2	91.4
D [21]	2.5	88.9	0.3	1.0	1.5	0.4	94.4
E [17]	4.3	87.3 ²			3.8		96.0
F [17]	4.0	83.0 ²			6.2		94.0

¹: $x_{Fe}/(x_{Fe}+x_{FeO})$; ²: DRI with high share of Fe₃C; n.a.: not available.

DRI and HBI are charged with steel scrap in varying amounts to the EAF, depending on local costs and availability. HBI is usually charged with the steel scrap by buckets to the EAF, requiring only minor adaptations to the EAF process at HBI shares up to 10%. Sidewall natural gas burners are of low importance for DRI melting as the maximum efficient energy transfer of gas burners is related to a solid scrap in the EAF. DRI is charged in cold or hot conditions to the EAF continuously via the 5th hole in the EAF roof, with charge weight portions from 50% to >95%. Depending on the particular EAF shell design, the remaining melt volume (hot heel) increases up to 30% of the total melt volume in order to facilitate the melting of the charged DRI (modern EAF shell designs exist even with a higher share of the hot heel). In these cases, the power programs must be adapted to continuous charging of material, long flat bath conditions, and increased input of lime and dololime for slag forming. The usual specific consumption figures of lime and dololime for scrap charged EAFs, 30–45 kg/t_{LS}, result in a specific amount of slag in the range of 70–100 kg/t_{LS}, according to the CaO mass balance (Equation (1) with $m_{DRI} = 0$). The total mass of slag per heat, m_{slag} , is determined by the CaO input with the slag formers (lime, dololime) and DRI neglecting a small loss of CaO to the off-gas system with EAF dust (Equation (1)):

$$x_{CaO,Lime} \cdot m_{Lime} + x_{CaO,Dololime} \cdot m_{Dololime} + x_{CaO,DRI} \cdot m_{DRI} = x_{CaO,Slag} \cdot m_{Slag}, m_i \text{ in kg or kg/t}_{LS}, x_i \text{ in wt \%} \quad (1)$$

With increased lime and dololime input for DRI heats in order to operate at standard slag basicity (x_{CaO}/x_{SiO_2}) in the range from 1.8–2.1 for minimum corrosion of the refractory lining, the specific amount and volume of the process slag are significantly increased up to 140 kg/t_{LS} (Equation (1)). The increased input of burned slag formers increases the electric energy demand accordingly by approx. 0.37–0.50 kWh/kg [22].

Continuous charging of raw materials provides EAF operation at flat bath conditions of a steel melt volume at a smoothly increasing level which benefits arc stability and control and decreased noise at the work floor. The absence of a scrap pile in the DRI-charged EAF, however, results in power programs with lower arc length, i.e., lower arc voltage, and slightly lower efficiency of energy transfer to the steel melt. Third, the metal yield of DRI charges is often lower, $m_{charged\ metal}/m_{tapped\ steel} = 87\text{--}92\%$, due to the oxide gangue in DRI compared with heats of 100% steel scrap with medium or high quality, 90–94%. As a result of these DRI-specific process conditions, the specific electrical energy demand of DRI heats is higher than for melting of steel scrap heats for carbon steel grades. The according melting time and tap-to-tap time of DRI heats is significantly longer than for scrap heats. EAF production characteristics of scrap heats vs. DRI heats are given in Table 2.

Table 2. Range of typical production parameters of electric arc furnace (EAF) charges with scrap and scrap/DRI, respectively, for low alloyed steel grades.

Charges Based on		100% Scrap	80–95% DRI
Share of DRI/HBI	(%)	0–5 (HBI)	60–95 (DRI)
Electric energy demand	(kWh/t)	340–390	530–680
Natural gas	(m ³ /t)	5–10	0–2
Oxygen	(m ³ /t)	25–37	20–35
Coal and carbon fines	(kg/t)	2–9	8–17
Slag former (lime, doloma, etc.)	(kg/t)	23–35	27–60
Tap temperature	(°C)	1600–1635	1600–1635
Tap-to-tap time	(min)	50–60	60–100
Metal yield	(%)	90–94	87–92

3. Increased Mass and Energy Efficiency by Controlled EAF Slag Operation

3.1. Slag Analysis as Helpful Tool to Monitor, Control and Improve EAF Operation

Besides control of arc length and, occasionally, of analysis of power harmonics [23], frequent slag sampling and analysis has been implemented as an efficient process monitoring tool in order to operate efficiently at foaming slag conditions with an appropriate slag viscosity that require a certain control of slag composition at MgO saturation [24–26]. In steelmaking processes with high generation rates of CO gas, e.g., increased share of pig iron, hot metal or DRI, the control of the slag composition is less important for slag foaming but for controlling the corrosion of the MgO-based lining caused by strongly MgO-undersaturated slags [21,27,28].

Examples of average slag compositions of EAF heats based on steel scrap charges and on charges with steel scrap and > 50% DRI are given in Table 3. Figures 1 and 2 visualize the distributions of slag composition with respect to MgO saturation [26]. The product portfolio covered rebar and construction steel grades (14 EAFs) to special steel grades (2 EAFs). The applied raw materials were steel scrap (EAF 1 to 8) and blends of steel scrap with 50% to 100% DRI (EAF 9 to 16). The sizes of the EAFs ranged from 60 t to >200 t tap weight, located in nine countries worldwide. Slag samples were taken from the EAFs shortly before tapping and analyzed at the steel plant laboratory. Only mislabeled slag data, e.g., those from transport ladles (i.e., FeO < 10% and CaO > 45%) or from raw materials (e.g., lime, DRI), were excluded from the data sets.

Besides controlling the slag basicity, e.g., $B_2 = x_{CaO}/x_{SiO_2}$ or $B_4 = (x_{CaO} + x_{MgO})/(x_{SiO_2} + x_{Al_2O_3})$, and MgO saturation, the control of FeO is important for avoiding unnecessary high Fe losses with the slag and increasing the metal yield; typical values are currently in the range of 25–30% FeO. Scatter of slag data provides information about the control on mass balance in the EAF, e.g., the appropriate input of CaO via lime and dolomite for SiO₂ compensation and controlled slag basicity. Variations of FeO content of the tapped slag indicate the quality of FeO control by carbon and oxygen injectors. There is evidence from slag analysis data in Table 3 that (1) the average Fe loss in DRI-charged EAFs is higher than for steel scrap heats, and (2) the control of FeO is more difficult for DRI-charged EAF heats. The standard deviation of FeO is in the range of 3.9–5.5 for heats based on steel scrap and 4.1–9.6 for heats based on steel scrap, and > 50% DRI. This is unexpected as DRI provides a more defined mass input to the EAF due to DRI production from iron ores and continuous monitoring of the DRI composition, in contrast to steel scrap with distinct quality classes and impurities. The lower control of slag compositions in DRI heats also seen in Figure 1 (heats based on steel scrap) vs. Figure 2 (heats based on > 50% DRI).

Table 3. Average slag compositions at the tapping of EAFs charged with steel scrap only and charged with scrap and > 50% DRI (slag compositions in wt %).

Scrap	#	CaO	SiO ₂	FeO	MgO	Al ₂ O ₃	MnO	Cr ₂ O ₃	Total ¹	σ FeO	Basicity	
EAF 1 ¹	422	26.1	16.7	29.5	10.5	8.4	5.6	1.6	99.6	4.1	1.6 ⁴	1.5 ⁵
EAF 2 ¹	359	31.1	11.6	28.1	10.6	5.4	5.0	1.1	94.4	4.6	2.7 ⁴	2.5 ⁵
EAF 3 ¹	1216	25.6	13.5	34.5	11.3	6.0	6.4	2.5	100.7	5.3	1.9 ⁴	1.9 ⁵
EAF 4 ¹	472	25.6	12.1	29.7	9.4	14.5	4.6	2.1	97.9	4.9	2.1 ⁴	1.3 ⁵
EAF 5 ²	149	27.3	8.8	40.2	8.3	3.5	7.0	3.2	99.4	5.2	3.1 ⁴	2.9 ⁵
EAF 6 ¹	424	28.4	12.6	36.2	3.8	8.7	9.6	n.a.	99.8	3.9	2.3 ⁴	1.5 ⁵
EAF 7 ¹	202	30.0	14.5	34.5	10.8	4.5	1.9	0.6	98.3	4.5	2.1 ⁴	2.1 ⁵
EAF 8 ¹	858	36.1	15.7	25.0	9.3	10.3	0.7	n.a.	97.5	4.0	2.3 ⁴	1.7 ⁵
DRI		CaO	SiO ₂	FeO	MgO	Al ₂ O ₃	MnO	TiO ₂	Total ²	σ FeO	Basicity	
EAF 9 ¹	132	27.0	16.0	31.1	14.9	6.0	1.9	1.2	98.0	8.3	1.7 ⁴	1.9 ⁵
EAF 10 ¹	29	39.2	16.6	31.8	5.4	5.9	1.4	n.a.	100.3	6.9	2.4 ⁴	2.0 ⁵
EAF 11 ¹	325	28.5	19.4	33.9	9.7	3.2	0.2	3.7	99.3	4.9	1.5 ⁴	1.7 ⁵
EAF 12 ¹	203	36.9	17.4	30.1	7.7	5.1	0.9	n.a.	95.5	5.5	2.1 ⁴	2.0 ⁵
EAF 13 ³	519	32.4	18.7	28.5	10.4	8.7	1.2	n.a.	99.8	4.7	1.7 ⁴	1.6 ⁵
EAF 14 ¹	19	40.5	17.7	21.7	9.4	6.7	1.9	0.8	99.2	9.6	2.3 ⁴	2.0 ⁵
EAF 15 ¹	918	30.5	21.0	26.3	11.3	5.2	1.2	n.a.	95.9	4.5	1.4 ⁴	1.6 ⁵
EAF 16 ¹	123	38.9	18.2	31.5	4.3	5.6	2.0	n.a.	100.4	6.2	2.1 ⁴	1.8 ⁵

¹: rebar and construction steel grades, ²: specialty steel grades, ³: construction and specialty steel grades; #: number of slag data; ⁴: $B_2 = \text{CaO}/\text{SiO}_2$; ⁵: $B_4 = (\text{CaO} + \text{MgO})/(\text{SiO}_2 + \text{Al}_2\text{O}_3)$, n.a.: not available, σ standard deviation.

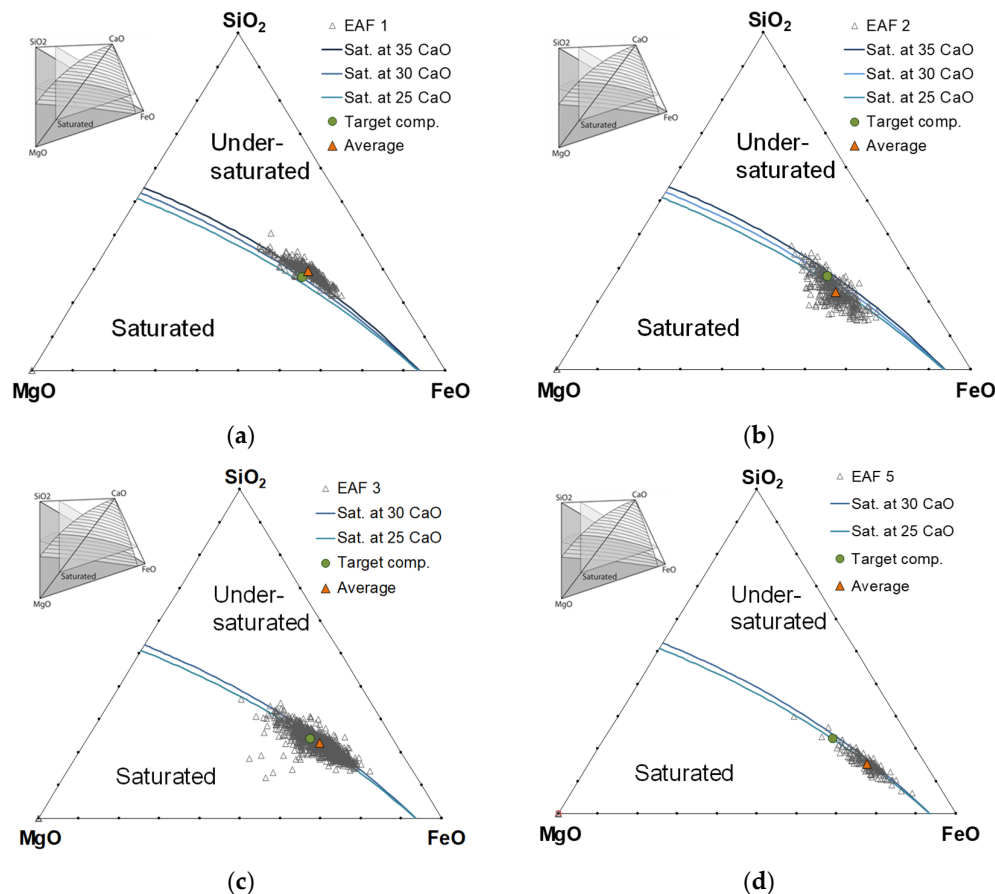


Figure 1. Distribution of slag analysis data from EAF heats for carbon steelmaking based on steel scrap (4 different EAFs (a–d)), in the system CaO–SiO₂–FeO–MgO–5% Al₂O₃; lines indicate MgO saturation at 25% to 35% CaO and 1600 °C [26].

3.2. Slag Characteristics of DRI-EAF Heats

The distribution of slag compositions for DRI heats is more complex than for heats based on steel scrap. In most cases, the EAF slags at tapping after melting and refining are close to the MgO saturation surface (Figure 1). This is due to the dissolution of MgO from the MgO-based EAF hearth and sidewall lining to the initial slag based on the remaining slag from the preceding heat and input of lime and dolomite. Precisely defined mixtures of lime and dolomite or another MgO-carrier provide an initial process slag closer to the MgO saturation with lower corrosion potential to the MgO hearth or MgO-C sidewalls (EAFs in Figure 1). Initial process slags based on lime or dolomitic lime only provide a higher corrosion potential (e.g., EAF 1 for scrap-based heats and EAF 11, and 12 for DRI-based heats in Table 3).

For DRI heats, the slag compositions show a more complex figure (Figure 2). The distribution and scatter of slag compositions at tapping are often higher than for scrap-based EAF heats. One reason is the EAF operation with an MgO-undersaturated initial slag if an MgO-carrier is not applied as slag former due to cost reasons or low availability of high-quality dolomite or dolomitic lime. In these cases, the slag compositions show final MgO concentrations between the initial slag composition and the MgO saturation surface (e.g., EAF 10, 11, 12 in Figure 2). EAF 11 displays an unusually large distribution of MgO concentrations due to losses of MgO gunning and hearth repair mixes to the slag. Remarkably, the average slag composition of EAF 11 seems to be close to MgO saturation, although the slag operation is rather out of control.

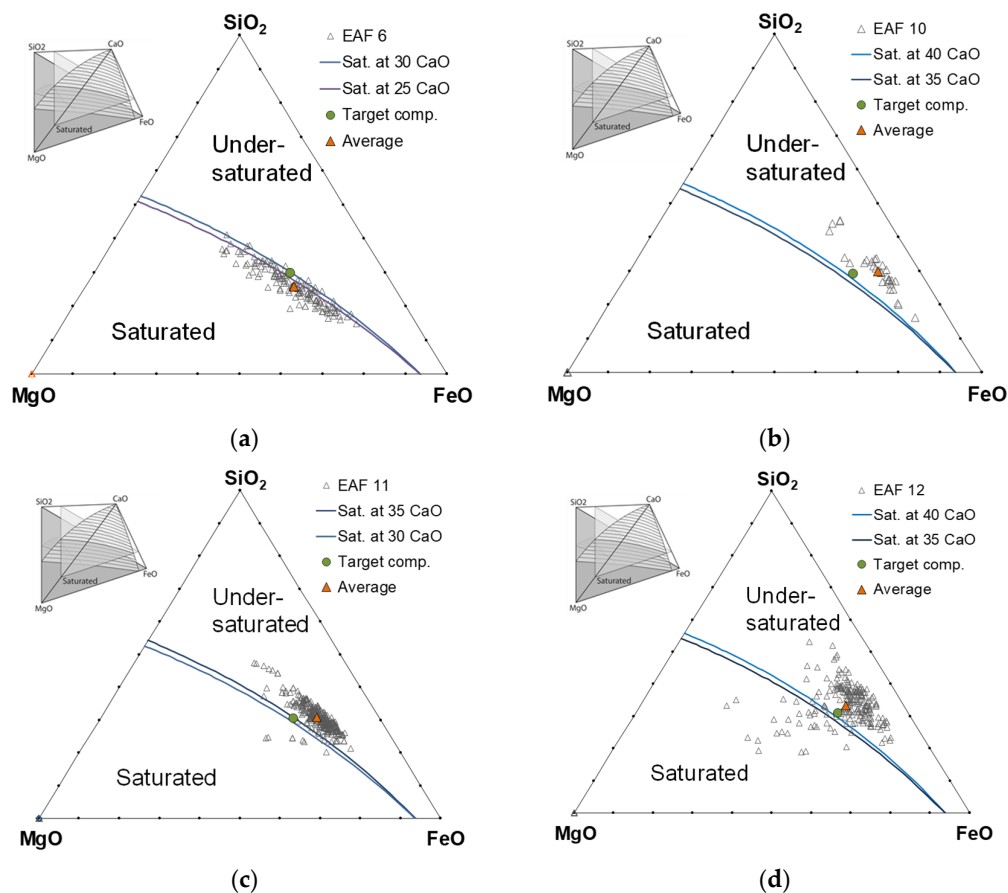


Figure 2. Distribution of slag analysis data from EAF heats for carbon steelmaking based on DRI (4 different EAFs (a–d)), in the system CaO–SiO₂–FeO–MgO–5% Al₂O₃; lines indicate MgO saturation at 25% to 40% CaO and 1600 °C.

Even more important for DRI-based heats is the control of FeO. Standard variation of FeO in Table 3 and the visual distribution of slag compositions in Figure 2 indicate a tendency to lower FeO control for DRI charges. Independent from basicity control, FeO ranges from 20 to > 45%. Even if the lime and dolomite input provides a more balanced process slag in order to operate at MgO saturated conditions (e.g., EAF 9 in Figure 2), the distribution of FeO at tapping is higher than usual. Recalling that composition control of DRI metallic raw material is usually better than for steel scrap due to better control on raw materials, continuous DRI production and usually DRI production on-site, low FeO control depends more likely on inappropriate EAF operation than on DRI input.

3.3. Slag Operation of DRI Heats at Lower Total Slag Mass

Specific slag masses are given in Figure 3, Equation (1), for heats based on steel scrap (up to 5% HBI) and DRI-based heats, assuming 2.5% SiO₂ and 0.5% CaO in DRI (Table 1) and 33% CaO in slag (Table 3). As the slag mass is higher for DRI heats due to the increased SiO₂ input, similar FeO concentration of the slag represents an elevated loss of Fe, approximately 0.9 kg/t_S Fe loss per% FeO in 120 kg/t slag (instead of 0.5 kg/t_S Fe loss per% FeO for steel scrap-based heats with lower slag mass, 70 kg/t). It is very likely that the lower control on FeO in the slag of DRI heats is due to the significantly increased slag volume that is continuously discharged from the EAF during the second half of DRI melting at elevated melt levels. Then, the retention time of the slag in the EAF is short, resulting in FeO levels with low control by carbon injectors or mixing with steel melt. With lower total slag volume, the discharging of slag starts at a later period of melting, providing an increased reduction of FeO by increased mixing with steel melt. Operating DRI heats at lower slag volume, however, requires lower input of lime, dolomite, i.e., EAF operation at lower basicity in the range $x_{CaO}/x_{SiO_2} = 1.6$ – 1.7 (Figure 3). In order to control and minimize corrosion of the MgO hearth and lining at low slag basicity, it is important to operate with slags near the MgO saturation from the very beginning by the adapted mass balance of lime and MgO carrier. MgO saturation can be efficiently monitored and controlled with diagrams in Figures 1 and 2 [26] or other saturation diagrams [23–25]. Some DRI-EAFs are operating at low basicity (EAF 9, 11, 13, 15 in Table 3), but half of the DRI-EAFs are still operating at high slag volumes and basicity near 2 (EAF 10, 12, 14, 16 in Table 3) following general EAF operating rules in order to minimize corrosion of the MgO lining and to operate at efficiently foaming slag in steel scrap charges. Due to increased input of carbon with DRI compared to steel scrap, CO formation is increased, and slag foaming is generally very well for DRI heats.

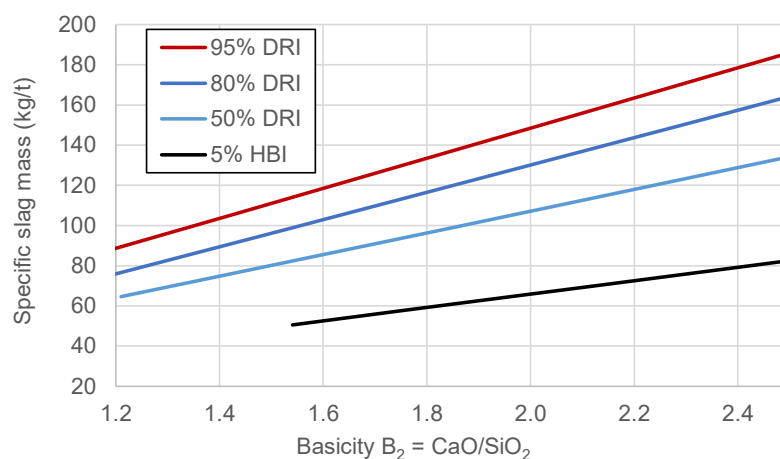


Figure 3. Specific slag volume as a function of slag basicity (x_{CaO}/x_{SiO_2}) for various ratios of DRI/hot briquetted iron (HBI) to steel scrap (assuming 2.5% SiO₂ and 0.5% CaO in DRI and 33% CaO in slag, Equation (1)).

4. EAF Process Modeling and Results.

The impact of a decreased use of slag formers on the energy efficiency of the EAF process was evaluated using a comprehensive process model for continuous charging of DRI developed from the EAF model for discontinuous charging of steel scrap proposed by Meier et al. [29–31] and described in previous publications [32,33].

4.1. Consistent Mass and Energy Balance Model for EAF Process

The model had to be adjusted for the DRI-based process since it has previously been developed and validated only for the scrap-based operation of EAF. The simulation was therefore adapted to accept a DRI feed rate instead of a scrap charge from a bucket. The DRI is added to the solid scrap zone in the model, and the parameters determining the heat transfer to the scrap zone were adjusted to account for the different behavior of the DRI compared to a pile of scrap melting down. Furthermore, while previously a SiO₂ and FeO content of the feed material could be set in addition to the Fe and trace elements, the significant gangue content of DRI necessitated the consideration of the CaO, MgO and Al₂O₃ content as well. The oxides are added to the liquid slag zone as the DRI melts. The option to define a mass flow of slag formers such as lime and dolomite was already present in the model and could therefore be used without additional adjustments. The de-slagging, however, was added by defining a mass flow that is removed from the liquid slag zone and increases with the height of the slag (being zero below a set threshold). Other parts of the model, such as the heat transfer and chemical models, mainly remained unchanged as the operation with DRI is mostly identical to the flat-bath phase of the scrap-based process.

The operation chart determining inputs such as the electrical power or the mass flows of oxygen and carbon fines was based on the operation of an industrial EAF with a 100% DRI charge. Additional inputs, as well as empirical model parameters and the furnace geometry, were estimated based on similar sized EAF for scrap melting, for which extensive validation data were available. Based on this operation chart, the input of lime and dolomite was both increased and decreased in 10% steps simulating an input from 70% to 150% of slag formers compared to the original industrial operation. The initial slag and hot heel composition were based on the average measured compositions available from the data, and the DRI composition was set according to measured values as well with a temperature of the charged DRI of 250 °C. Hot heel and initial slag mass and the beginning of the heat were estimated, and the parameters determining the de-slagging rate and the heating and melting rates of the DRI were adjusted so that all DRI is melted by the end of the heat and the slag amount remaining is similar to the initial slag mass as would be expected for the continuous operation of the furnace.

While the model has been extensively validated using process data from scrap-based operations [29–31,33] and remains mostly unchanged, the data available for this study was limited to the average operation chart and compositions already mentioned as well as tapping temperatures for three heats with the time of measurements given as within 3–5 min before tapping. Therefore, only the general temperature range, as well as qualitative results such as the already mentioned expected melting of all DRI and amount of slag produced and removed from the furnace, were available for validation of the model results. As the aim of this study is only a rough estimation and qualitative evaluation of the impact of the number of slag formers used in the process, this is, however, considered to be sufficient.

4.2. Results—Implications on Energy Balance, Savings and Productivity

As expected, the results showed the energy demand for the same tapping temperature increasing with a higher amount of slag formers charged. The adapted electrical energy input was adjusted by increasing or decreasing the power-on time of the same power program accordingly. Additionally, the basicity ratio changes as expected for

the constant amount of DRI and therefore SiO_2 charged and varying amounts of CaO delivered from the added lime and dolomite. The results of the simulations are summarized in Figure 4 concerning savings in power-on time and specific electrical energy demand by decreasing the lime and dolomite input.

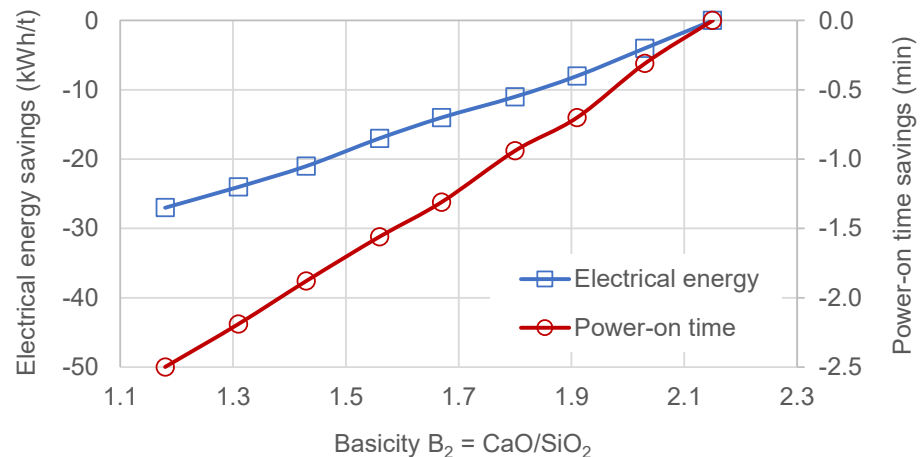


Figure 4. Calculated influence of lime and dolomite input via slag basicity on power-in time and electrical energy demand of a 100% DRI-charged EAF model.

5. Discussion

Increased use of DRI in the EAF process increases the input of SiO_2 with DRI gangue oxides. An adapted EAF slag operation from standard basicity $x_{\text{CaO}}/x_{\text{SiO}_2} = 2.0$ to lower basicity values in the range 1.4 to 1.7 decreases the total slag mass and corresponding FeO loss to the slag as well as the electrical energy demand by approx. 8–17 kWh/t and consequently the power-on time. At lower slag basicity, however, the increased MgO saturation concentrations must be considered, e.g., by adapted saturation figures (Figure 2 [26]), in order not to increase the wear rate of the MgO lining. Due to the lower total slag mass, the efficiency of FeO reduction by carbon injection may be improved. In addition, the FeO losses by slag during DRI charging may be decreased: whereas dense HBI is usually charged with steel scrap by buckets to the EAF at minor amounts, DRI is charged continuously with or besides slag formers via the 5th hole in the EAF roof. Commercially produced DRI tends to form fines due to its high porosity [34]. Usually, the feeding spot is chosen near or between the electrodes (often between electrodes one and two near the slag door). Charged pellets fall into the steel melt due to the increased density of the reduced material (3.5–3.9 g/cm³ [35]), whereas DRI fines stick to the slag layer above the steel melt.

Both the contamination of the slag samples with unreacted DRI fines and decreased efficiency of carbon injectors could be explanations of the observed increased FeO variation of slags from DRI charges in contrast to steel scrap charges (Table 3). An alternative DRI feeding spot between electrodes two and three (opposite to the slag door) could provide a longer retention time of DRI fines in the EAF for improved reduction of FeO residuals. Adapted oxygen injector positions may be necessary for an optimized DRI feeding spot.

The adapted EAF mass and energy model indicates differences between scrap charges and DRI charges due to different oxides input and flat bath conditions, e.g., improved slag foaming due to the carbon content of the DRI in agreement with common observation at DRI-EAFs. However, further improvements to the model are necessary in order to investigate the details of the DRI charging spot.

Author Contributions: Conceptualization, methodology, analysis of slag data, M.K.; modeling, software, validation, T.H., T.E.; writing, M.K., T.H., T.E.; All authors have read and agreed to the published version of the manuscript.

Funding: The APC was funded by the German Research Foundation (DFG) and the University of Bayreuth in the funding program Open Access Publishing.

Conflicts of Interest: The authors declare no conflicts of interest.

References

1. Wörtler, M.; Schuler, M.; Voigt, N.; Schmidt, T.; Dahmann, P.; Lungen, H.B.; Ghenda, J.T. Steel's contribution to a low-carbon Europe 2050. In *Technical and Economic Analysis of the Sector's CO₂ Abatement Potential*; The Boston Consulting Group, Steel Institute VDEh: Boston, FL, USA, 2013.
2. Toktarova, A.; Karlsson, I.; Rootzén, J.; Göransson, L.; Odenberger, M.; Johnsson, F. Pathways for Low-Carbon Transition of the Steel Industry—A Swedish Case Study. *Energies* **2020**, *13*, 3840, doi:10.3390/en13153840.
3. Pardo, N.; Moya, J.A. Prospective scenarios on energy efficiency and CO₂ emissions in the European Iron & Steel industry. *Energy* **2013**, *54*, 113–128, doi:10.1016/j.energy.2013.03.015.
4. Ravenscroft, C.M.; Howell, R.W.; Bonelli, G. Building a bigger DRI plant: Expanding operational flexibility with responsible and reliable scale-up of new 2.5 Mtpy MIDREX[®] cDRI/hDRI plants in Algeria. In Proceedings of the Association for Iron and Steel Technology Conference Proceedings 2018 (AISTech 2018), Philadelphia, PA, USA, 7–10 May 2018; pp. 715–723.
5. Formanek, L.; Lungen, H.B.; Pröls, J.; Rose, F.; Stellmacher, U. Iron, Chapter 3. Direct Reduction Processes. In *Ullmann's Encyclopedia of Industrial Chemistry*; Wiley-VCH Verlag GmbH & Co.: Hoboken, NJ, USA, 2019. doi:10.1002/14356007.o14_o02.pub3.
6. Memoli, F.; Kemper, K. The Innovative DRI-EAF Route for the Production of High-Purity Pig Iron. In Proceedings of the Association for Iron and Steel Technology Conference Proceedings 2018 (AISTech 2018), Philadelphia, PA, USA, 7–10 May 2018; pp. 625–632.
7. Dey, N.R.; Prasad, A.K.; Singh, S.K. Energy survey of the coal based sponge iron industry. *Case Stud. Therm. Eng.* **2015**, *6*, 1–15.
8. Vishal, G.; Choudhary, P.; Deo, B.; Sahoo, S.K.; Malakar, P.; Pothal, G.; Chattopadhyay, P. Optimal control of accretion growth and quality of sponge iron in a coal-fired rotary kiln at Tata Sponge, India. In Proceedings of the Association for Iron and Steel Technology Conference Proceedings 2018 (AISTech 2018), Philadelphia, PA, USA, 7–10 May 2018; pp. 773–780.
9. Mehl, S. Sustainable Technologies for Small, Mid and Large-Scale Iron Ore Pellet Production and Mid-Scale DRI. In Proceedings of the Iranian Iron & Steel Conference, Kish, Iran, 14–16 September 2015.
10. Kekkonen, M.; Holappa, L. Comparison of different coal-based direct reduction processes. In *Helsinki University of Technology Publications in Materials Science and Metallurgy*; Report TTK-MK-99; Helsinki University: Espoo, Finland, 2000; ISBN 951-22-5134-5.
11. Sawa, Y.; Yamamoto, T.; Takeda, K.; Itaya, H. New coal-based process to produce high quality DRI for the EAF. *ISIJ Int.* **2001**, *41*, S17–S21.
12. Meijer, K.; Borlee, J.; Skorianz, M.; Feilmayr, C.; Goedert, P.; Dry, R. HIsarna—Highly Energy-Efficient Ironmaking. In Proceedings of the Association for Iron and Steel Technology Conference Proceedings 2015 (AISTech 2015), Cleveland, OH, USA, 4–7 May 2015; pp. 1116–1122.
13. Song, J.; Jiang, Z.; Bao, C.; Xu, A. Comparison of Energy Consumption and CO₂ Emission for Three Steel Production Routes—Integrated Steel Plant Equipped with Blast Furnace, Oxygen Blast Furnace or COREX. *Metals* **2019**, *9*, 364, doi:10.3390/met9030364.
14. The Intergovernmental Panel on Climate Change. *2006 IPCC Guidelines for National Greenhouse Gas Inventories, Volume 3: Industrial Processes and Product Use, Chapter 4: Metal Industry Emissions*; The Intergovernmental Panel on Climate Change: Geneva, Switzerland, 2006.
15. Rammer, B.; Millner, R.; Boehm, C. Comparing the CO₂ Emissions of Different Steelmaking Routes. *Berg Hüttenmänn. Monatsh.* **2017**, *162*, 7–13, doi:10.1007/s00501-016-0561-8.
16. World Steel Dynamics. *2019 World Direct Reduction Statistics*; World Steel Dynamics: Englewood Cliffs, NJ, USA, 2020; pp. 1–15.
17. Memoli, F. Behavior and Benefits of High-Fe₃C DRI in the EAF. In Proceedings of the Association for Iron and Steel Technology Conference Proceedings 2015 (AISTech 2015), Cleveland, OH, USA, 4–7 May 2015; pp. 1928–1945.
18. Chevrier, V. MIDREX H₂—Ultimate Low-CO₂ Ironmaking and Its Place in the New Hydrogen Economy. In Proceedings of the Association for Iron and Steel Technology Conference Proceedings 2018 (AISTech 2018), Philadelphia, PA, USA, 7–10 May 2018; pp. 725–729.
19. Kirschen, M.; Badr, K.; Pfeifer, H. Influence of direct reduced iron on the energy balance of the electric arc furnace in steel industry. *Energy* **2011**, *36*, 6146–6155, doi:10.1016/j.energy.2011.07.050.
20. Memoli, F.; Jones, J.A.T.; Picciolo, F.; Palamini, N. The use of DRI in a Consteel[®] EAF Process. *Iron Steel Technol.* **2015**, *12*, 72–80.
21. Song, S.; Zhao, J.; Pistorius, P.C. MgO refractory attack by transient non-saturated EAF slag. *Metall. Mater. Trans. B* **2020**, *51*, 891, doi:10.1007/s11663-020-01788-x.

22. Pfeifer, H.; Kirschen, M.; Simoes, J.P. Thermodynamic analysis of electrical energy demand. In Proceedings of the 8th European Electric Steelmaking Conference, London, UK, 9–12 May 2005; The Institute of Materials, Minerals and Mining IOM3 Conference Communications; pp. 211–232.
23. Vieira, D.; de Almeida, R.A.M.; Bielefeldt, W.A.; Vilela, A.C.F. Slag Evaluation to Reduce Energy Consumption and EAF Electrical Instability. *Mater. Res.* **2016**, doi:10.1590/1980-5373-MR-2015-0720.
24. Pretorius, E.B.; Carlisle, R. Foamy slag fundamentals and their practical application to electric furnace steelmaking. *Iron Steelmak.* **1999**, *26*, 79–88.
25. Pretorius, E.B. Slag Fundamentals. An Introduction to the Theory and Practice of EF Steelmaking. *Iron Steel Soc.* **1998**, *26*, 79–88.
26. Kirschen, M. Visualization of Slag Data for Efficient Monitoring and Improvement of Steelmaking Slag Operation in Electric Arc Furnaces, with a Focus on MgO Saturation. *Metals* **2021**, *11*, 17, doi:10.3390/met11010017.
27. Patrizio, D.; Razza, P.; Pesamosca, A. Capacity enhancement at Emirates Steel: Continuous improvement in EAF performance with hot DRI Charge. In Proceedings of the Association for Iron and Steel Technology Conference Proceedings 2015 (AISTech 2015), Cleveland, OH, USA, 4–7 May 2015; pp. 1954–1964.
28. López, F.; Farrando, A.; López, M.; Picco, L.; Loeffelholz, M. Slag modeling for optimizing the use of fluxes in a DRI-based steelmaking operation. In Proceedings of the Association for Iron and Steel Technology Conference Proceedings 2016 (AISTech 2016), Pittsburgh, PA, USA, 16–19 May 2016; pp. 875–880.
29. Meier, T.; Gandt, K.; Hay, T.; Echterhof, T. Process Modeling and Simulation of the Radiation in the Electric Arc Furnace. *Steel Res. Int.* **2018**, *89*, 1700487.
30. Meier, T.; Hay, T.; Echterhof, T.; Pfeifer, H.; Rekersdrees, T.; Schlinge, L.; Elsabagh, S.; Schliephake, H. Process Modeling and Simulation of Biochar Usage in an Electric Arc Furnace as a Substitute for Fossil Coal. *Steel Res. Int.* **2017**, *88*, 1600458, doi:10.1002/srin.201600458.
31. Meier, T. Modellierung und Simulation des Elektrolichtbogenofens. Ph.D. Thesis, RWTH Aachen University, Aachen, Germany, 2016.
32. Hay, T.; Echterhof, T.; Visuri, V.V. Development of an Electric Arc Furnace Simulator Based on a Comprehensive Dynamic Process Model. *Processes* **2019**, *7*, 852, doi:10.3390/pr7110852.
33. Hay, T.; Reimann, A.; Echterhof, T. Improving the Modeling of Slag and Steel Bath Chemistry in an Electric Arc Furnace Process Model. *Metall. Mater. Trans. B* **2019**, *50*, 2377–2388, doi:10.1007/s11663-019-01632-x.
34. Kim, G.; Pistorius, P.C. Strength of Direct Reduced Iron Following Gas-Based Reduction and Carburization. *Metall. Mater. Trans. B* **2020**, *51*, 2628–2641, doi:10.1007/s11663-020-01958-x.
35. Monsen, B.E.; Thomassen, E.S.; Bragstad, I.; Ringdalen, E.; Hoegaas, P.H. Characterization of DR Pellets for DRI Applications. In Proceedings of the Association for Iron and Steel Technology Conference Proceedings 2015 (AISTech 2015), Cleveland, OH, USA, 4–7 May 2015; pp. 739–750.